

# Multiferroic domain relaxation in $(\text{NH}_4)_2[\text{FeCl}_5(\text{H}_2\text{O})]$

S. Biesenkamp,<sup>1</sup> K. Schmalzl,<sup>2</sup> P. Becker,<sup>3</sup> L. Bohatý,<sup>3</sup> and M. Braden<sup>1, \*</sup>

<sup>1</sup>*II. Physikalisches Institut, Universität zu Köln, Zùlpicher Straße 77, D-50937 Köln, Germany*

<sup>2</sup>*Juelich Centre for Neutron Science JCNS, Forschungszentrum Juelich GmbH, Outstation at ILL, 38042 Grenoble, France*

<sup>3</sup>*Institut für Geologie und Mineralogie, Abteilung Kristallographie, Universität zu Köln, Zùlpicher Straße 49b, 50674 Köln, Germany*

(Dated: August 30, 2023)

The molecular compound  $(\text{NH}_4)_2[\text{FeCl}_5(\text{H}_2\text{O})]$  is a type-II multiferroic material, in which incommensurate cycloidal order directly induces ferroelectric polarization. The multiferroic domain kinetics in  $(\text{NH}_4)_2[\text{FeCl}_5(\text{H}_2\text{O})]$  were studied by time-resolved neutron diffraction experiments utilizing neutron polarization analysis. The temperature and electric-field dependent multiferroic relaxation obeys the simple combined Arrhenius-Merz law, which was reported to describe domain kinetics in the prototype multiferroics  $\text{TbMnO}_3$  and  $\text{NaFeGe}_2\text{O}_6$ . However, the characteristic time scale of the multiferroic relaxation is considerably larger than those in  $\text{TbMnO}_3$  or  $\text{NaFeGe}_2\text{O}_6$ . Temperature-dependent diffraction on  $(\text{NH}_4)_2[\text{FeCl}_5(\text{H}_2\text{O})]$  reveals the emergence of higher-order and commensurate magnetic contributions upon cooling in the multiferroic phase in zero field. The good agreement with studies of higher-harmonic contributions in the deuterated material indicates that the isotopes only possess a minor impact on the magnetic ordering. But in contrast to similar observations in multiferroic  $\text{MnWO}_4$ , this anharmonic modification of magnetic ordering does not depin multiferroic domain walls or alter the temperature dependence of the multiferroic relaxation.

## I. INTRODUCTION

The control of complex magnetic and electric ordering parameters by external electric or magnetic fields stimulates the research on multiferroic materials [1–3]. Especially type-II multiferroics attract much interest, as improper ferroelectric ordering is not only coexisting with magnetic ordering but is also induced by it [1]. This inherently entails strong magneto-electric coupling and an application potential in low-power memory devices [3]. The inverse Dzyaloshinskii-Moriya interaction (DMI) [4, 5] drives the multiferroic state in most type-II multiferroics. The canting of neighboring spins in spirals induces a shift of non-magnetic ions in between and thus a ferroelectric polarization, whose sign depends on the handedness of the spiral [6]. An external electric field can thus control the sign of the vector chirality of the spiral spin structure.

Recent studies of multiferroic domain inversion revealed that the relaxation in  $\text{TbMnO}_3$  and  $\text{NaFeGe}_2\text{O}_6$  follows a simple combined Arrhenius-Merz law suggesting thermally activated domain-wall motion [7, 8]. In the general Arrhenius activation, the dynamics of a process is described by  $\exp(-\frac{E_A}{k_B T})$  or by a relaxation time following  $\tau \propto \exp(\frac{E_A}{k_B T})$  with  $E_A$  the activation energy. In a ferroelectric material the electric field can control and invert the domains, and in many compounds the dependence of this relaxation on the electric field follows the Merz law at constant temperature,  $\tau \propto \exp(\frac{F_A}{E})$  where  $F_A$  is an activation field [9]. However, in proper ferroelectric switching, the nucleation at the surface, their subsequent forward growth along the polarization direction

and finally the sideways growth of needle shaped domains act on the same time scale [9] rendering the temperature dependence difficult to describe. In contrast, the multiferroic domain inversion is mostly dominated by the sideways growth of some few large domains [7, 10–12]. In  $\text{TbMnO}_3$  and in  $\text{NaFeGe}_2\text{O}_6$  the combination of both relations well describes the multiferroic relaxation over many decades in time. The combined Arrhenius-Merz relation is expressed as:

$$\tau(E, T) = \tau^* \exp\left(\frac{A_0 T_r}{ET}\right) \text{ with } T_r = \frac{T_{\text{MF}} - T}{T_{\text{MF}}}. \quad (1)$$

In this relation there are only two independent parameters: an activation constant  $A_0$  and a critical relaxation time  $\tau^*$  that is reached by either increasing the electric field to infinity or by approaching the multiferroic transition,  $T_r = 0$ . The observation of such a simple relation over many time decades indicates a single slow process to dominate the multiferroic relaxation, i.e. the growth of a few large domains by domain wall motion. Furthermore, the critical relaxation time  $\tau^*$  must correspond to some intrinsic entity that does not change in the multiferroic phase. It is tempting to identify  $\tau^*$  with the inverse of the spin-wave velocity, but the effective distance the domain growth must cover is neither known nor controlled.

There is at least one exception to this relation. The domain inversion in multiferroic  $\text{MnWO}_4$  is peculiar as it speeds up upon cooling towards the lower boundary of the multiferroic phase where the incommensurate order transforms into a commensurate one [11, 13, 14]. Magnetic correlations in  $\text{MnWO}_4$  start to resemble the commensurate spin up-up-down-down (*uudd*) arrangements already in its incommensurate multiferroic phase, as tiny commensurate fragments occur. Therefore, the interference of commensurate and incommensurate ordering can

\* e-mail: braden@ph2.uni-koeln.de

depin multiferroic domains and thus cause the speeding up of multiferroic domain inversion near the lower first-order magnetic transition [15]. The different relaxation behavior motivates the investigation of multiferroic domain inversion in other materials, in particular in a molecular compound, which promises a softer nuclear lattice.

The erythrosiderites  $A_2[\text{FeCl}_5(\text{H}_2\text{O})]$  with  $A$  being an ammonium or an alkali-metal ion have attracted much interest as some members exhibit magnetoelectric and even multiferroic behavior [16, 17]. Structurally, erythrosiderites are closely related to each other. The magnetic  $\text{Fe}^{3+}$  ion is surrounded by 5  $\text{Cl}^-$  ions and the O of the water molecule  $\text{H}_2\text{O}$ . These  $\text{FeCl}_5\text{H}_2\text{O}$  octahedra are not directly connected (no shared ligands) but separated by the  $A$  ions. The hydrogen of the  $\text{H}_2\text{O}$  ligands, however, provides bonding between O and Cl ions of neighboring octahedra. Considering these H-bridge bonds the  $\text{FeCl}_5\text{H}_2\text{O}$  octahedra form zigzag chains. However, the alignment of these zigzag chains differs in the material class between  $A = \text{Cs}$  and the others ( $A = \text{NH}_4, \text{Rb}, \text{K}$ ) [18–23]. The latter compounds crystallize in space group  $Pnma$  with chains along  $b$ , see Fig. 1, and the H-bonds are fully determined by the general arrangement. In contrast for  $A = \text{Cs}$ , there is a structural phase transition, at which these bonds order [24]. Most erythrosiderites were reported to develop antiferromagnetic and collinear magnetic structures at low temperatures [25–27], whereby the easy axis points along the  $a$  direction. However, this does not hold for the ammonium compound, for which an  $ac$  easy plane with  $XY$  anisotropy was observed [28, 29].

Orthorhombic  $(\text{NH}_4)_2[\text{FeCl}_5(\text{H}_2\text{O})]$  (space group  $Pnma$ ) exhibits the unit cell dimensions  $a = 13.706(2) \text{ \AA}$ ,  $b = 9.924(1) \text{ \AA}$  and  $c = 7.024(1) \text{ \AA}$  [16, 30] at room temperature. At  $T_S \approx 79 \text{ K}$  a structural order-disorder transition of the tetrahedral  $(\text{NH}_4)^+$  groups leads to the loss of  $n$  and  $m$  symmetries and thus to a monoclinic distortion of the crystal lattice [28, 31]. Below  $T_S$  the system can be described by space group  $P2_1/a$  (non-standard setting) and no further symmetry reductions are reported at low temperature [31]. At  $T_N \approx 7.3 \text{ K}$  long-range magnetic order in the form of an incommensurate spin density wave (SDW) with moments along the  $a$  direction sets in [16, 28, 29]. The propagation vector  $\mathbf{k} = (0 \ 0 \ 0.23)$  displays a slight temperature dependence but it does not reach a commensurate value [29]. Below the multiferroic transition at  $T_{\text{MF}} \approx 6.8 \text{ K}$  a spiral spin structure forms with moments rotating in the  $ac$  plane [28, 29] and ferroelectric polarization of  $\approx 3 \mu\text{C}/\text{m}^2$  emerges [16]. The substitution of the protons by deuterium slightly enhances the structural transition by about one Kelvin but has no measurable impact on the two magnetic transitions [31]. Note, that the ferroelectric polarization arising from the magnetic ordering was only determined for the proton material [16]. The inverse DMI well explains multiferroic coupling in  $(\text{NH}_4)_2[\text{FeCl}_5(\text{H}_2\text{O})]$ . However, Tian *et al.* reported that the groundstate is not homogeneous but consists

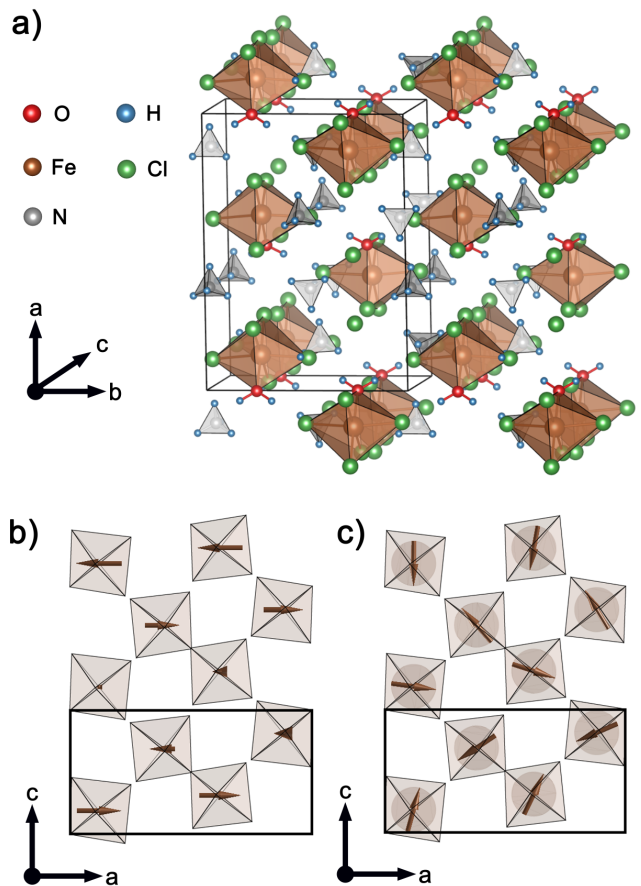


FIG. 1. Panel a) displays the crystal structure of  $(\text{NH}_4)_2[\text{FeCl}_5(\text{H}_2\text{O})]$  with ordered  $(\text{NH}_4)^+$  tetrahedra, whereby the respective structural data were taken from the low-temperature refinement in Ref. 31. For the visualization of the crystallographic parts the software VESTA3 [32] was utilized. In b) and c), the magnetic structure of both phases, the intermediate SDW phase and the low-temperature spiral multiferroic phase are sketched within the  $ac$  plane. The magnetic structure information was taken from Ref. 28 and Ref. 29.

of two soft phases in form of incommensurate and commensurate ordering [33]. In zero magnetic field, incommensurate ordering predominates but at a magnetic field along  $a$  of  $\approx 2.5 \text{ T}$  the structure transforms into a distorted commensurate cycloid [33, 34], and at  $\approx 5 \text{ T}$  a spin-flop transition induces a commensurate canted spin structure with moments lying mainly within the  $bc$  plane [16, 34]. The ferroelectric polarization at zero field has its main component along the  $a$  direction with a ten times smaller component along  $b$  [16]. At the first transition in magnetic fields the polarization tilts slightly away from the  $a$  direction, and above the spin-flop transition the ferroelectric polarization points along the  $c$  direction. This orientation of ferroelectric polarization disagrees with the DMI mechanism but can be described by the spin dependent  $p$ - $d$  hybridization model [16, 34]. The interfering of incommensurate and

commensurate ordering in the multiferroic phase as well as the molecular character promise different relaxation processes and motivate the investigation of the domain kinetics in  $(\text{NH}_4)_2[\text{FeCl}_5(\text{H}_2\text{O})]$ .

In the following sections we first introduce the experimental methods before presenting time-resolved polarized neutron-diffraction studies of multiferroic domain inversion in  $(\text{NH}_4)_2[\text{FeCl}_5(\text{H}_2\text{O})]$ . The temperature and electric field dependence of relaxation times follows again the combined Arrhenius-Merz relation given in equation 1 [7]. In addition, we discuss the temperature dependence of the commensurate correlations and that of higher harmonic reflections and their possible impact on the relaxation behavior.

## II. EXPERIMENTAL METHODS

For the investigation of the multiferroic domain dynamics and for sensing the handedness of the spiral spin structure, neutron diffraction with polarization analysis was utilized. As the molecular compound  $(\text{NH}_4)_2[\text{FeCl}_5(\text{H}_2\text{O})]$  contains hydrogen atoms, which cause a strong incoherent background, previous magnetic neutron-scattering experiments were performed only on deuterated samples [28, 29, 31, 33–35]. Polarized neutron diffraction does not significantly profit from the reduced background signal, and as the handling of deuterated samples is complicated we prepared two non-deuterated samples (SI and SII), with dimensions of about  $3.8 \text{ mm} \times 4.8 \text{ mm} \times 1.03 \text{ mm}$  for SI and  $5.2 \text{ mm} \times 5.8 \text{ mm} \times 3.1 \text{ mm}$  for SII. An elaborate description of the sample growth can be found in Ref. 16. Both crystals were clamped between aluminium plates that are tightened together by insulating polytetrafluorethylen (PTFE) screws. The plate normal was oriented parallel  $a$  in order to apply the electric field along the predominant component of the ferroelectric polarization. Both plates were mounted on separate sample holders in the scattering geometry  $(0\ 1\ 0)/(0\ 0\ 1)$  and connected to the high-voltage setup. This setup contains two ISEG modules (BPP4W and BPN4W), which provide a maximum output voltage of plus and minus 4 kV, respectively, and a MOSFET array (BEHLKE HTS-111) that is capable to switch periodically between both polarities within less than  $50 \mu\text{s}$  (for a detailed description of this setup see Ref. 7) generating a nearly rectangular time shape of the electric-field profile. The time-resolved measurements are realized with a multichannel data collector (MESYTEC MCPD-8), which records neutrons in event mode with a timestamp. After the data recording single neutron events are distributed to the discrete time dependency  $I([t_i, t_i + \Delta t])$  with a time binning  $\Delta t$  that can still be adapted. Very fast relaxation processes can be resolved, because the statistics only depend on the number of switching periods and hence can be increased at any order. For measuring quasistatic hysteresis loops, while driving the applied electric field between its extrema, a FUG HCP 14-3500 high-voltage generator was

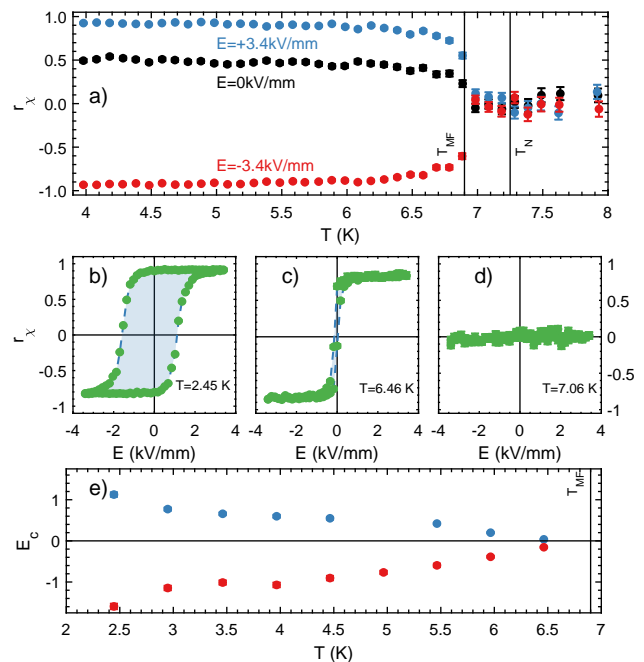


FIG. 2. The temperature dependence of the chiral ratio for different poling fields is displayed in a). Panels b), c) and d) show three exemplary hysteresis loops at  $T = 2.45 \text{ K}$ ,  $T = 6.46 \text{ K}$  and  $T = 7.06 \text{ K}$ . The coercive fields were obtained by fitting both slopes with a hyperbolic tangent and the respective temperature dependence is shown in e). All measurements were recorded for the  $\mathbf{Q} = (0\ 1\ 0.23)$  reflection.

used.

The time-resolved investigations of the multiferroic domain inversion were carried out at the triple-axis spectrometer IN12 at the Institute Laue-Langevin (ILL) [36]. A pyrolytic graphite (PG(002)) monochromator supplied  $\lambda = 3.14 \text{ \AA}$ , while a cavity polarizer provided a highly polarized neutron beam. The sample was inserted in a standard orange cryostat and a Helmholtz-coil setup defined the guide-field direction at the sample position. Two spin flippers that are positioned before and behind the sample as well as a Heusler (111) analyzer enabled longitudinal polarization analysis. The flipping ratio (FR) was measured on the  $(0\ 2\ 0)$  nuclear reflection and amounts to  $\text{FR} \approx 20$ .

For measuring the temperature dependence of the higher harmonics, we carried out an experiment at the IN3 triple-axis spectrometer at the ILL. A PG (002) monochromator provided an unpolarized neutron beam with  $\lambda = 2.36 \text{ \AA}$  and the background signal was significantly reduced by a PG (002) analyzer. With the standard orange cryostat, the temperature dependence of higher harmonics was measured down to  $T = 1.5 \text{ K}$ .

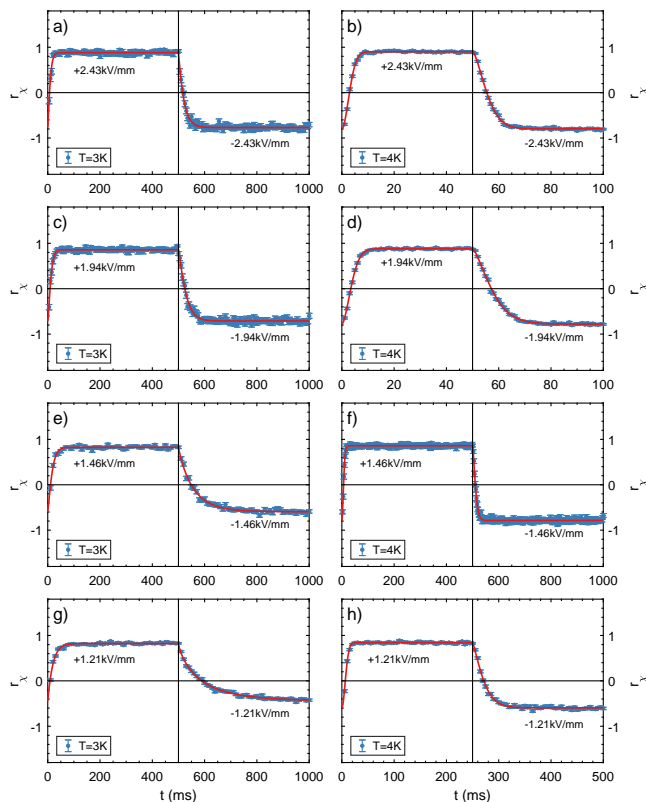


FIG. 3. Multiferrroic switching curves are plotted in panels a)-h) for different temperatures and electric field amplitudes. These measurements were performed on sample SI and by recording both SF channels  $I_{x\bar{x}}$  and  $I_{\bar{x}x}$  for the magnetic reflection  $\mathbf{Q} = (0 \ 1 \ 0.23)$ .

### III. MULTIFERRROIC DOMAIN CONTROL

For the temperature and electric field dependent investigation of the multiferrroic domain dynamics, sample SI was measured at the IN12 triple-axis spectrometer utilizing longitudinal polarization analysis. Unpolarized neutron diffraction senses the Fourier transform of the magnetization perpendicular to the scattering vector  $\mathbf{M}_\perp$  yielding a magnetic intensity contribution proportional to  $|\mathbf{M}_\perp|^2$ . Without neutron polarization, there is no interference between nuclear and magnetic structures, but, for a polarized neutron beam, additional terms need to be considered [37]. Since we are studying purely magnetic Bragg peaks, there is no nuclear magnetic interference, but the chiral term,  $i(\mathbf{M}_\perp \times \mathbf{M}_\perp^*)_x$ , causes magnetic cross sections that depend on the sign of the neutron polarization both before and after the scattering process. We use the common coordinate system in polarized neutron diffraction, where  $\mathbf{x}$  is along the scattering vector  $\mathbf{Q}$ ,  $\mathbf{y}$  perpendicular to  $\mathbf{Q}$  in the scattering plane and  $\mathbf{z} = \mathbf{x} \times \mathbf{y}$ . The chiral term can be studied by measuring both spin-flip (SF) channels  $I_{x\bar{x}}$  and  $I_{\bar{x}x}$  yielding the chiral ratio  $r_\chi = (I_{x\bar{x}} - I_{\bar{x}x}) / (I_{x\bar{x}} + I_{\bar{x}x}) = \pm i(\mathbf{M}_\perp \times \mathbf{M}_\perp^*)_x / |\mathbf{M}_\perp|^2$ . The sign of the chiral contri-

bution senses the sign of the vector chirality and thus the handedness of the spin spiral. In an ideal scattering geometry with  $\mathbf{Q}$  perpendicular to the envelope of the chiral magnetic structure and assuming a circular rotation of magnetic moments, a chiral ratio of  $\pm 1$  is expected for a monodomain state. If the scattering vector is not perfectly perpendicular to the rotation plane of spins or if the spiral is elliptically distorted, the maximum value of  $r_\chi$  is reduced, but rather large deformations are required to yield a significant deviation of the expectation  $r_\chi = 1$  for a monodomain state.

In the first part of the experiment, the chiral ratio was measured at  $\mathbf{Q} = (0 \ 1 \ 0.23)$  as a function of temperature and for different applied electric fields. For each run, the sample was heated above the Néel temperature and subsequently cooled with applied electric field, while recording both SF channels  $I_{x\bar{x}}$  and  $I_{\bar{x}x}$ . In Fig. 2 a) the temperature dependence of  $r_\chi$  is shown for  $E = \pm 3.4$  kV/mm as well as for zero applied field. The values clearly state that the sign of the vector chirality can be poled in opposite directions depending on the applied field direction and even close to the multiferrroic transition temperature the system can be poled to a monodomain state. Moreover, it can be seen that in zero field a finite value for  $r_\chi$  develops, which indicates a preferred state of the multiferrroic domain distribution for this sample. In consequence, multiferrroic domains at zero electric field should already be rather large.

The temperature dependence of the chiral ratio shown in Fig. 2 a) nicely agrees with that of the ferroelectric polarization [16], as it is expected for the inverse Dzyaloshinski-Moriya coupling. Both sense the product of the two orthogonal spin components of the cycloidal structure. Upon cooling, both quantities exhibit a small jump at  $T_{\text{MF}}$  and then further increase in the multiferrroic phase.

Hysteresis loops were recorded by quasistatically driving the applied electric field between  $E = \pm 3.4$  kV/mm for different temperatures. Three exemplary loops are shown in Fig. 2 b)-d). The hysteresis loops confirm the invertibility of the spiral handedness in  $(\text{NH}_4)_2[\text{FeCl}_5(\text{H}_2\text{O})]$  by external electric fields, while the visible asymmetry of the coercive fields agrees with the results from the poling sequences. Figure 2 e) presents the temperature dependence of the coercive fields  $E_c$  obtained by fitting both slopes of the hysteresis loop by a hyperbolic tangent. The quasistatic measurements resemble those on a deuterated sample [34], which however revealed smaller values of the chiral ratios. Upon cooling through the multiferrroic transition with applied field we find  $r_\chi = 0.920(6)$  and also in the hysteresis a high value is reached at the favorite side,  $r_\chi = 0.92(1)$ . For a perfect circular envelope and a monodomain state one expects an ideal chiral ratio of 1 that is reduced by the finite flipping ratio to  $r_\chi = 0.91$  in perfect agreement with the observations. The alignment of multiferrroic domains is thus perfect within a few percent.

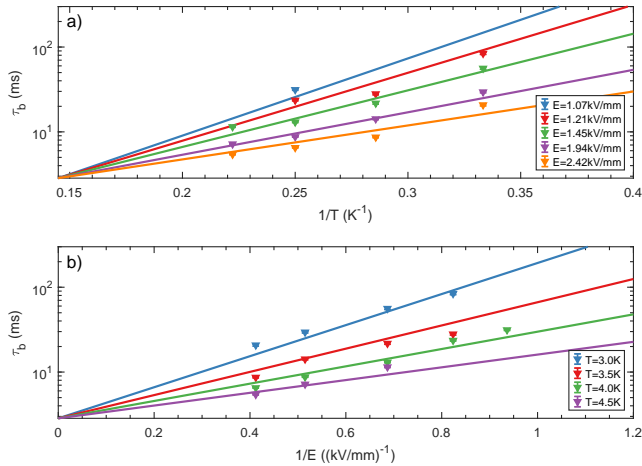


FIG. 4. Both panels a) and b) display the determined relaxation time on a logarithmic scale as a function of inverse temperature and inverse electric-field amplitude. Because of the observed asymmetry, the relaxation time is plotted only for one switching direction (here  $\tau_b$ ). Solid lines refer to the fit result for respective temperatures and fields.

#### IV. RELAXATION BEHAVIOR

The relaxation times of multiferroic domain inversion as a function of temperature and electric field were determined by deploying the time-resolved setup (see Ref. 7) at the IN12 spectrometer. These measurements were performed on the same sample and on the same position in Q space as for the quasi-static measurements. Figure 3 displays exemplary switching curves that were recorded for different temperatures and electric field amplitudes. It can be seen that the inversion time for these switching curves cover more than one order of magnitude as a function of temperature and electric field. Furthermore, the observed preference of one domain population becomes evident by the asymmetry of the switching curve. In analogy to the analysis in Ref. 7 and Ref. 8 the rising and falling parts of all switching curves were fitted by stretched exponential functions:

$$r_\chi(t) = r_a - (r_a - r_b) \exp\left(-\left(\frac{t}{\tau_a}\right)^{b_1}\right) \quad (2)$$

$$r_\chi(t) = r_b - (r_b - r_a) \exp\left(-\left(\frac{t - t_{1/2}}{\tau_b}\right)^{b_2}\right) \quad (3)$$

These functions describe the relaxation process from state  $r_b$  to state  $r_a$  and vice versa with relaxation times  $\tau_a$  and  $\tau_b$ , respectively. The value  $t_{1/2}$  denotes the switching time of the external field at half the period. Following the Ishibashi and Takagi theory [38, 39], which relies on the Avrami model for phase change kinetics [40–42], both exponential factors  $b_1$  and  $b_2$  indicate the domain

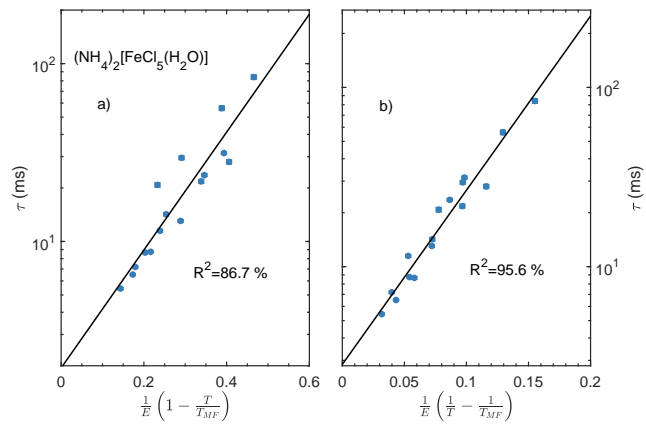


FIG. 5. The different scaling concepts for the temperature and electric-field dependent multiferroic domain inversion are compared. Panel a) displays the relaxation times plotted against the argument  $\frac{1}{E} \left(1 - \frac{T}{T_{MF}}\right) = \frac{T_r}{E}$  that is observed in some ferroelectric materials, and panel b) shows the scaling with the argument  $\frac{1}{E} \left(\frac{1}{T} - \frac{1}{T_{MF}}\right) = \frac{T_r}{ET}$  predicted by the Arrhenius-Merz combination, see equation 1. Quantitative agreement factors are included.

growth dimensionality for respective switching directions. Fitting all switching curves with equation 2 and 3 yield  $b$  parameters in the range between 1 and 2, which indicates low dimensional domain growth. Furthermore, the  $b$  values tend to raise for increased field or temperature. This is expected as for higher temperatures or higher electric fields the assumption of only a few nuclei forming at the beginning transforms into a continuous growth of nuclei during the switching process. An equivalent behavior was observed for  $\text{TbMnO}_3$  and  $\text{NaFeGe}_2\text{O}_6$  [7, 8].

All fitted relaxation times are shown in Fig. 4 as a function of inverse temperature and inverse electric field. For the sake of simplicity, only  $\tau_b$  is plotted as both relaxation times  $\tau_a$  and  $\tau_b$  differ approximately by a factor of 2-3 due to the observed asymmetry of domain inversion (see Fig. 3). However, the following discussion is qualitatively the same for both directions. The electric-field and temperature dependence of the multiferroic relaxation time in  $(\text{NH}_4)_2[\text{FeCl}_5(\text{H}_2\text{O})]$  follows again the combined Arrhenius-Merz law (Equation 1). Fitting all determined relaxation times with Equation 1 yields the values  $A_0 = 22.4(14) \text{ K kV/mm}$  and  $\tau^* = 2.85(31) \text{ ms}$  for the multiferroic domain relaxation in  $(\text{NH}_4)_2[\text{FeCl}_5(\text{H}_2\text{O})]$ . The measured relaxation times cover two orders of magnitude in time as a function of temperature and electric field. Astonishingly, the fastest resulting relaxation time  $\tau^*$  in molecular  $(\text{NH}_4)_2[\text{FeCl}_5(\text{H}_2\text{O})]$  is one order of magnitude slower than that in  $\text{TbMnO}_3$  [7] and more than two orders of magnitude slower than that in  $\text{NaFeGe}_2\text{O}_6$  [8]. However, this has to be set in relation to the multiferroic transition temperature and to the activation constant.  $\text{TbMnO}_3$  exhibits a much higher transition temperature and the two order of magnitude larger activa-

tion constant  $A_0$  tremendously slows down the relaxation process at low temperature. In the multiferroic temperature range of  $(\text{NH}_4)_2[\text{FeCl}_5(\text{H}_2\text{O})]$ , the  $\text{TbMnO}_3$  domain inversion is thus much slower. The multiferroic transition temperature of  $\text{NaFeGe}_2\text{O}_6$  is higher than that in  $(\text{NH}_4)_2[\text{FeCl}_5(\text{H}_2\text{O})]$ , whereas the activation constant is smaller. Therefore, the relaxation in this oxide system is still faster compared to  $(\text{NH}_4)_2[\text{FeCl}_5(\text{H}_2\text{O})]$ , when considering the same temperature range. The molecular constituents in  $(\text{NH}_4)_2[\text{FeCl}_5(\text{H}_2\text{O})]$  thus do not imply faster relaxation.

For  $\text{NaFeGe}_2\text{O}_6$  the critical relaxation time  $\tau^*$  and thus the fastest possible multiferroic domain inversion agrees with the order of magnitude of the spin wave velocity [8],  $v_{sw} \sim 1000$  m/s. The inversion of the multiferroic domains is associated with the inversion of the chirality of cycloidal order. Among the several low-energy magnons in such a cycloidal arrangement, the phason modes and their spin-wave velocity seem most related to such an effect [43, 44]. Also for  $(\text{ND}_4)_2[\text{FeCl}_5(\text{D}_2\text{O})]$  the magnon dispersion was studied by inelastic neutron experiments revealing spin-wave velocities of the same order of magnitude in the multiferroic phase [45]. However, it is important to emphasize that in an antiferromagnetic material with a spin gap, spin-wave velocities can be deduced only away from the incommensurate magnetic zone centers. Right at the zone center, the magnon dispersion becomes flat and the derivative  $\frac{dE}{dq}$  depends on the propagation vector. Therefore, the effective spin-wave velocity being relevant for the multiferroic domain relaxation can be much slower than that observed in the magnetic Brillouin zone. A detailed determination of the spin gap associated with the phason branch was only reported for multiferroic  $\text{TbMnO}_3$  [43, 44]. Although the phason excitations extend to very low energies of the order of 0.1 meV, the phason right at the zone center exhibits a clear tail to larger energies that can arise from the interplay between Mn and Tb moments. A larger gap of the phason branch in  $(\text{NH}_4)_2[\text{FeCl}_5(\text{H}_2\text{O})]$  or in any other multiferroic material can induce a much flatter magnon dispersion and thus a much smaller effective spin-wave velocity that slows the relaxation down. Further high-resolution inelastic neutron scattering experiments on  $(\text{NH}_4)_2[\text{FeCl}_5(\text{H}_2\text{O})]$  and other type-II multiferroic materials are highly desirable. The existing data on  $\text{TbMnO}_3$  [7],  $\text{NaFeGe}_2\text{O}_6$  [8] and  $(\text{NH}_4)_2[\text{FeCl}_5(\text{H}_2\text{O})]$  already exclude a simple relation between  $\tau^*$  and the spin-wave velocities at larger propagation vector.

The validity of the combined Arrhenius-Merz relation is confirmed by the implied scaling of the relaxation time  $\tau = f(T_r/(ET))$ , which is displayed in Fig. 5 b). Scaling against the argument of the Arrhenius-Merz relation is well fulfilled down to low temperature. In contrast, the relation  $\tau = f(T_r/E)$  proposed for proper ferroelectrics [9] yields stronger deviations, see Fig. 5 a). There is no indication for a failure of the relation at the lowest studied temperatures. In particular relaxation times are not getting shorter as one expects for either depinning of do-

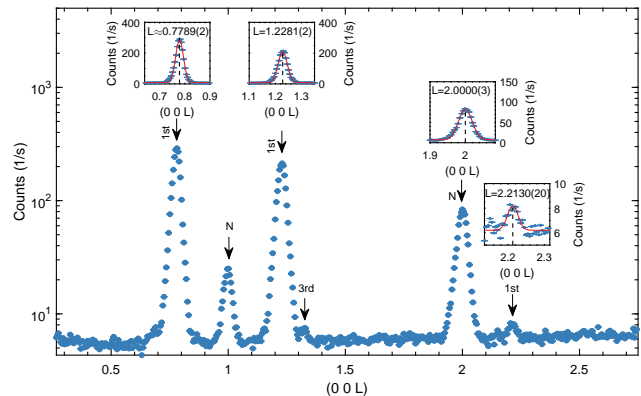


FIG. 6.  $Q_L$ -scan across  $(0\ 0\ L)$  direction at  $T = 1.48\text{K}$ . The observed nuclear (N), magnetic first order (1st) and magnetic third order (3rd) reflections are marked by arrows and the shown insets present Gaussian fits for some of the incommensurate first order and nuclear reflections, whereby the value of the fitted peak position is respectively included in all panels. An equivalent scan for the deuterated compound at  $T = 1.5\text{K}$  can be found in Ref. [29].

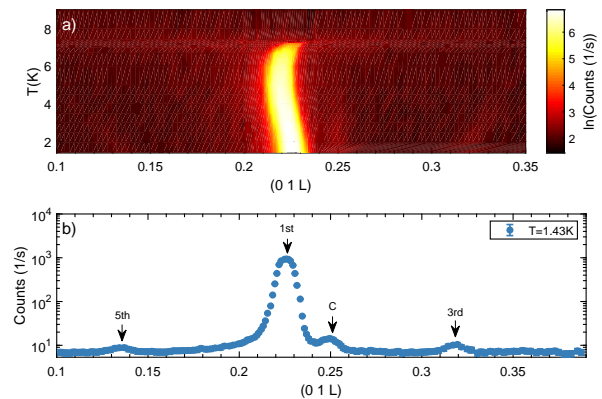


FIG. 7. The upper panel a) shows a temperature dependent  $Q_L$  scan across the magnetic reflection  $Q = (0\ 1\ 0.23)$ . One single scan is shown in panel b) for  $T = 1.43\text{K}$ , where first (1st), third (3rd), fifth (5th) order harmonics and commensurate (C) contributions are marked by arrows.

main walls or for the occurrence of quantum mechanical tunneling phenomena [46, 47].

## V. HIGHER HARMONICS

Tian *et al.* reported the competition of various ordering schemes  $(\text{ND}_4)_2[\text{FeCl}_5(\text{D}_2\text{O})]$ : incommensurate modulations with even and odd harmonics as well as a commensurate ordering appearing at low temperature ( $T = 1.5\text{K}$ ) [29, 33]. The interference of incommensurate and commensurate ordering can depin multiferroic domain walls and was suggested to cause the anomalous relaxation behavior in  $\text{MnWO}_4$  [11, 13–15]. Tian *et al.*

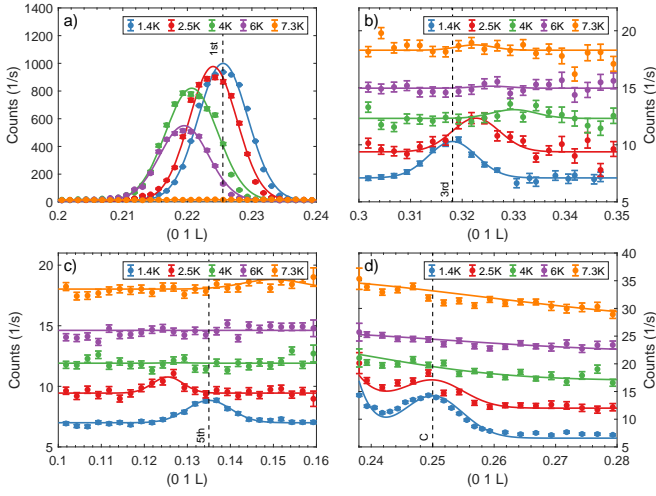


FIG. 8. The observable reflections from  $L$  scans and the respective fits. The first, third and fifth order reflections are respectively plotted in a)-c) together with a Gaussian fit, for which a constant background was assumed. This contrasts the fit of the commensurate reflection, which is displayed in d). Here, the background was assumed to be the tail of a second Gaussian function and the commensurate peak position was fixed to  $L = 0.25$ . For a better view, all respective scans in b)-d) are shifted by a constant offset with respect to the y-axis.

utilized neutron polarization analysis to separate the respective magnetic and nuclear contributions. Odd order harmonics and the commensurate signal are solely of magnetic origin, whereas the second order reflection is mainly of nuclear origin but possesses also a finite magnetic contribution [29]. This closely resembles the occurrence and origin of even and odd harmonics in  $\text{MnWO}_4$  [15, 48], in particular the double, nuclear and magnetic, character of the second order modulation. The appearance of second-order harmonics is rather common, because every incommensurate magnetic modulation implies a nuclear lattice modulation of half the period in real space due to exchange striction. Higher order contributions were also studied in other multiferroics [49–51] as well as in  $\text{Ba}_3\text{NbFe}_3\text{Si}_2\text{O}_{14}$  that is not multiferroic but exhibits a monodomain chiral magnetic structure inscribed by its non-centrosymmetric crystal structure [52]. In all these materials, the 3rd order contributions show peculiar temperature dependencies with a positive curvature that do not follow the temperature dependence of the first-order intensities. Moreover, in  $(\text{ND}_4)_2[\text{FeCl}_5(\text{D}_2\text{O})]$  and similarly in  $\text{MnWO}_4$  [15, 48] the reported temperature dependence revealed a strong enhancement of second order intensity with the onset of ferroelectric and chiral magnetic ordering, which indicates significant magnetoelastic coupling in the multiferroic phase. The observed third and fifth order harmonics signal a squaring up of the spin spiral. This was also observed in  $\text{MnWO}_4$  as a precursor of the low-temperature commensurate spin *uudd* phase. In  $(\text{ND}_4)_2[\text{FeCl}_5(\text{D}_2\text{O})]$ , no commensurate

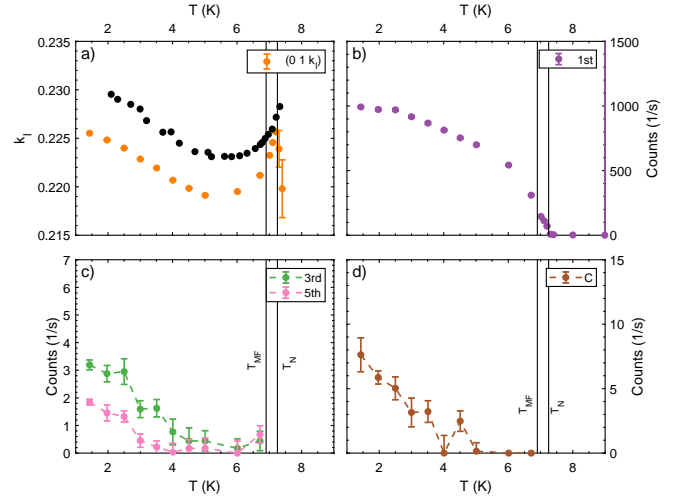


FIG. 9. Results from temperature dependent fits of all harmonic and commensurate reflections. Panel a) displays the obtained temperature dependence of the measured incommensurate propagation vector (orange data points) and compares it with data (black data points) from Ref. [29] obtained on a deuterated sample. The plots in b)-d) show the temperature dependent intensity of the 1st, 3rd, 5th harmonics as well as that of the commensurate (C) reflection for  $(\text{NH}_4)_2[\text{FeCl}_5(\text{H}_2\text{O})]$ .

low-temperature phase was so far reported but even harmonics and a sizable peak intensity for the commensurate reflection  $\mathbf{Q} = (0\ 1\ 0.25)$  in the incommensurate multiferroic phase indicate that commensurate order coexists and competes with the incommensurate ordering [29]. The incommensurate ordering is dominant in zero field but the coexisting commensurate ordering can be stabilized with increasing magnetic field, which leads to an intermediate region between 1.5 T-2.5 T before the spin spiral becomes commensurate and distorted at 2.5 T [29, 33, 34]. So far only the temperature dependence of even harmonics in the deuterated material was reported [29, 33], but to assess the impact of interfering commensurate and incommensurate ordering on the multiferroic relaxation behavior, temperature dependent measurements of odd harmonics and of the commensurate contributions are required.

Figure 6 presents a  $Q_L$ -scan across  $Q = (0\ 0\ L)$  in  $(\text{NH}_4)_2[\text{FeCl}_5(\text{H}_2\text{O})]$ , which was measured at the lowest temperature  $T = 1.48\ \text{K}$  and which resembles the respective measurement from Tian et al. [29] on the deuterated sample. As already suggested by the lack of isotope effect for the magnetic transition temperatures [31], this suggests a minor role of the isotope for the magnetic ordering. Nevertheless, some finite impact of the isotope on the magnetic structure is observed and will be described below. In both compounds, nuclear as well as magnetic first- and third-order reflections exhibit finite intensity at this temperature. The three incommensurate first order reflections in Fig. 6 are fitted by single Gaussian functions to determine their exact position and

thus the incommensurability of the underlying magnetic structure. The weighted average of determined values for the incommensurability yields the propagation vector  $k_{\text{inc}} = (0 \ 0 \ 0.2245(5))$ , which differs by approximately 2.5% from the one, which was reported for the deuterated sample [29]. This difference cannot be related to a potential misalignment of the sample as the observed nuclear reflections  $(0 \ 0 \ 2)$  is observed exactly at the expected position  $L = 2.0000(3)$  (see Gaussian fit in the right inset of Fig. 6).

Temperature-dependent scans are shown in Fig. 7 a), whereby Fig. 7 b) displays an exemplary single scan at  $T = 1.5\text{K}$ . This scan clearly confirms the reported presence [29] of odd harmonics and also the coexistence of incommensurate and commensurate reflections in the hydrogen system. We find a significantly smaller commensurate contribution that can be quantified by the ratio of  $(0 \ 1 \ 0.225)$  and  $(0 \ 1 \ 0.25)$  peaks, which amounts to  $\sim 5\%$  in the deuterated compound [29] and to less than one percent in the hydrogen crystal. The coexistence of the commensurate phase seems thus to be sample dependent, and most likely the enhanced disorder of the deuterated sample stabilizes a larger commensurate contribution.

All peaks were fitted separately by Gaussian functions, whereby a constant background was assumed for all higher harmonics. In contrast, for the commensurate reflection a second Gaussian function was used to describe the background, respectively the superimposed signal from the first order signal. These fits are shown in Fig. 8. The peak center position gives the value  $k_l$  for the incommensurate propagation vector  $k_{\text{inc}} = (00k_l)$ . Its temperature dependence is compared with the reported values from a deuterated sample [29] in Fig. 9 a) and obviously, both values for the incommensurability along  $c$  differ approximately by 2% in the entire temperature range. An isotope effect was so far reported only for the structural order-disorder transition temperature  $T_S = 79\text{K}$ , while isotope exchange does not significantly change the magnetic transition temperatures [31].

For assessing the intensity of higher harmonic reflections and hence the magnitude of anharmonic contributions to the spiral ordering, the related first order intensity is plotted in Fig. 9 b) as a function of temperature. In Fig. 9 c) the temperature dependencies of both odd higher harmonics are shown. The third order reflection evolves below  $T \sim 6\text{K}$ , whereas the fifth order reflection develops only below  $T \sim 4\text{K}$ . These intensities are of the same order of magnitude and they saturate at low temperature. By considering the geometry factor, it turns out that the peak intensity at  $T = 1.5\text{K}$  amounts to approximately  $10^{-3}$  of the incommensurate first order reflection, wherefore these odd harmonics can be estimated to be even relatively stronger than those in  $\text{MnWO}_4$  [15]. The related squaring up of spins enforces tiny commensurate fragments which is further indicated by the simultaneous development of a commensurate reflection (see Fig. 9)). However, the interfering commensurate ordering does not affect the relaxation behavior above  $T = 3\text{K}$

(see Fig. 4).

The main difference between  $(\text{NH}_4)_2[\text{FeCl}_5(\text{H}_2\text{O})]$  and  $\text{MnWO}_4$  [15] is the fact that odd harmonics and the development of tiny commensurate fragments appear at much lower temperature in the molecular compound. The pinning strength at lower temperature is naturally stronger and is thus capable to compensate the depinning effects from interfering commensurate ordering. Further, the intensity of odd harmonics in  $\text{MnWO}_4$  diverges at the lower transition to commensurate order [15], whereas in  $(\text{NH}_4)_2[\text{FeCl}_5(\text{H}_2\text{O})]$  the respective intensity follows the intensity of the incommensurate first order peak and saturates at low temperature. This behavior agrees with the absence of a transition to pure commensurate ordering at low temperature in  $(\text{NH}_4)_2[\text{FeCl}_5(\text{H}_2\text{O})]$ . It is thus expected that depinning effects do not significantly grow at much lower temperatures in  $(\text{NH}_4)_2[\text{FeCl}_5(\text{H}_2\text{O})]$ , which explains that the relaxation behavior agrees with the combined Arrhenius-Merz law even in the presence of some interfering commensurate ordering at  $3\text{K}$ .

$\text{TbMnO}_3$  is another multiferroic material, whose domain relaxation was studied [7], and it also exhibits the appearance of higher order contributions [49–51], but the use of rather large crystals in the neutron experiments prohibits a quantitative analysis, see the discussion in Ref. [44].

## VI. CONCLUSION

The multiferroic domain relaxation and the temperature dependence of magnetic correlations were studied in the molecular system  $(\text{NH}_4)_2[\text{FeCl}_5(\text{H}_2\text{O})]$  on a hydrogen-containing crystal, in contrast to most reported neutron diffraction experiments on this system analyzing deuterated crystals [28, 29, 31, 33–35]. The analysis of the hydrogen-containing sample reveals a slight isotope effect on the incommensurability of the magnetic structure. In addition the commensurate ordering coexisting at low temperature with the main incommensurate structure is considerably suppressed compared to measurements on deuterated samples. As deuteration intrinsically induces some disorder both effects can essentially stem from these perturbations.

Over a significant field and temperature range, the temperature and electric-field dependence of multiferroic relaxation in  $(\text{NH}_4)_2[\text{FeCl}_5(\text{H}_2\text{O})]$  follows the simple combined Arrhenius-Merz relation. The domain kinetics in the molecular compound are thus similar to the relaxation behavior in the previously studied oxide systems  $\text{TbMnO}_3$  and  $\text{NaFeGe}_2\text{O}_6$  [7, 8], but astonishingly, the relaxation in the molecular system is much slower than in  $\text{NaFeGe}_2\text{O}_6$  in spite of similar transition temperatures and similar spin-wave velocities indicating that other quantities, such as the spin gap, also play an important role.



## VII. ACKNOWLEDGEMENTS

This work was funded by the Deutsche Forschungsgemeinschaft (DFG, German Research Foundation) - Project number 277146847 - CRC 1238, projects A02 and B04. The neutron scattering data from the IN12 and IN3 diffractometer are available [53].

- 
- [1] D. Khomskii, Classifying multiferroics: Mechanisms and effects, *Physics* **2**, 20 (2009).
- [2] N. A. Spaldin and R. Ramesh, Advances in magnetoelectric multiferroics, *Nat. Mater.* **18**, 203 (2019).
- [3] J. F. Scott, Multiferroic memories, *Nat. Mater.* **6**, 256 (2007).
- [4] I. E. Dzyaloshinskii, A thermodynamic theory of “weak” ferromagnetism of antiferromagnetics, *J. Phys. Chem. Solids* **4**, 241 (1958).
- [5] T. Moriya, Anisotropic Superexchange Interaction and Weak Ferromagnetism, *Phys. Rev.* **120**, 91 (1960).
- [6] M. Mostovoy, Ferroelectricity in Spiral Magnets, *Phys. Rev. Lett.* **96**, 067601 (2006).
- [7] J. Stein, S. Biesenkamp, T. Cronert, T. Fröhlich, J. Leist, K. Schmalzl, A. C. Komarek, and M. Braden, Combined arrhenius-merz law describing domain relaxation in type-ii multiferroics, *Phys. Rev. Lett.* **127**, 097601 (2021).
- [8] S. Biesenkamp, D. Gorkov, W. Schmidt, K. Schmalzl, Y. Sidis, P. Becker, L. Bohatý, and M. Braden, Chiral order and multiferroic domain relaxation in  $\text{NaFeGe}_2\text{O}_6$ , *Phys. Rev. B* **104**, 174405 (2021).
- [9] J. F. Scott, *Ferroelectric Memories*, Advanced microelectronics (Springer, 2000).
- [10] D. Meier, N. Leo, M. Maringer, T. Lottermoser, M. Fiebig, P. Becker, and L. Bohatý, Topology and manipulation of multiferroic hybrid domains in  $\text{MnWO}_4$ , *Phys. Rev. B* **80**, 224420 (2009).
- [11] T. Hoffmann, P. Thielen, P. Becker, L. Bohatý, and M. Fiebig, Time-resolved imaging of magnetoelectric switching in multiferroic  $\text{MnWO}_4$ , *Phys. Rev. B* **84**, 184404 (2011).
- [12] M. Matsubara, S. Manz, M. Mochizuki, T. Kubacka, A. Iyama, N. Aliouane, T. Kimura, S. L. Johnson, D. Meier, and M. Fiebig, Magnetoelectric domain control in multiferroic  $\text{TbMnO}_3$ , *Science* **348**, 1112 (2015).
- [13] M. Baum, J. Leist, T. Finger, K. Schmalzl, A. Hiess, L. P. Regnault, P. Becker, L. Bohatý, G. Eckold, and M. Braden, Kinetics of the multiferroic switching in  $\text{MnWO}_4$ , *Phys. Rev. B* **89**, 1 (2014).
- [14] D. Niermann, C. P. Grams, M. Schalenbach, P. Becker, L. Bohatý, J. Stein, M. Braden, and J. Hemberger, Domain dynamics in the multiferroic phase of  $\text{MnWO}_4$ , *Phys. Rev. B* **89**, 134412 (2014).
- [15] S. Biesenkamp, N. Qureshi, Y. Sidis, P. Becker, L. Bohatý, and M. Braden, Structural dimerization in the commensurate magnetic phases of  $\text{NaFe(WO}_4)_2$  and  $\text{MnWO}_4$ , *Phys. Rev. B* **102**, 144429 (2020).
- [16] M. Ackermann, D. Brüning, T. Lorenz, P. Becker, and L. Bohatý, Thermodynamic properties of the new multiferroic material  $(\text{NH}_4)_2[\text{FeCl}_5(\text{H}_2\text{O})]$ , *New Journal of Physics* **15**, 123001 (2013).
- [17] M. Ackermann, T. Lorenz, P. Becker, and L. Bohatý, Magnetoelectric properties of  $A_2[\text{FeCl}_5(\text{H}_2\text{O})]$  with  $A = \text{K, Rb, Cs}$ , *Journal of Physics: Condensed Matter* **26**, 506002 (2014).
- [18] I. Lindqvist, The crystal structure of  $(\text{NH}_4)_2(\text{FeCl}_5(\text{H}_2\text{O}))$ , *Arkiv Kemi Mineral.* **24**, 1 (1946).
- [19] D. Lacková, I. Ondrejkočiová, and M. Koman, A new pathway of preparation and refined structure of  $(\text{NH}_4)_2[\text{FeCl}_5(\text{H}_2\text{O})]$ , *Acta Chimica Slovaca* **6**, 129 (2013).
- [20] B. N. Figgis, C. L. Raston, R. P. Sharma, and A. H. White, Crystal structure of diammonium aquapentachloroferrate(III), *Australian Journal of Chemistry* **31**, 2717 (1978).
- [21] C. J. O’Connor, B. S. Deaver, and E. Sinn, Crystal structures of  $A_2\text{FeCl}_5 \times \text{H}_2\text{O}$  ( $A = \text{Rb}^+, \text{Cs}^+$ ) and field dependent superconducting susceptometer measurements, *The Journal of Chemical Physics* **70**, 5161 (1979).
- [22] J. E. Greedan, D. C. Hewitt, R. Faggiani, and I. D. Brown, Structure of and hydrogen bonding in dicaesium aquapentachloroferrate(III), *Acta Crystallographica Section B* **36**, 1927 (1980).
- [23] A. J. Schultz and R. L. Carlin, Single-crystal pulsed neutron diffraction structure of the antiferromagnet  $\text{K}_2[\text{FeCl}_5(\text{H}_2\text{O})]$  with and without applied pressure, *Acta Crystallographica Section B* **51**, 43 (1995).
- [24] T. Fröhlich, J. Stein, L. Bohatý, P. Becker, A. Gukasov, and M. Braden, Structural and magnetic phase transitions in  $\text{Cs}_2[\text{FeCl}_5(\text{H}_2\text{O})]$ , *Journal of Physics: Condensed Matter* **30**, 295403 (2018).
- [25] M. Gabas, F. Palacio, J. Rodríguez-Carvajal, and D. Visser, Magnetic structures of the three-dimensional Heisenberg antiferromagnets  $\text{K}_2\text{FeCl}_5 \cdot \text{D}_2\text{O}$  and  $\text{Rb}_2\text{FeCl}_5 \cdot \text{D}_2\text{O}$ , *Journal of Physics: Condensed Matter* **7**, 4725 (1995).
- [26] J. Campo, J. Luzón, F. Palacio, G. J. McIntyre, A. Millán, and A. R. Wildes, Understanding magnetic interactions in the series  $A_2\text{FeX}_5 \cdot \text{H}_2\text{O}$  ( $A = \text{K, Rb}$ ;  $X = \text{Cl, Br}$ ). II. Inelastic neutron scattering and DFT studies, *Phys. Rev. B* **78**, 054415 (2008).
- [27] J. Luzón, J. Campo, F. Palacio, G. J. McIntyre, and A. Millán, Understanding magnetic interactions in the series  $A_2\text{FeX}_5 \cdot \text{H}_2\text{O}$  ( $A = \text{K, Rb}$ ;  $X = \text{Cl, Br}$ ). I. Spin densities by polarized neutron diffraction and DFT calculations, *Phys. Rev. B* **78**, 054414 (2008).
- [28] J. Alberto Rodríguez-Velamazán, O. Fabelo, A. Millán, J. Campo, R. D. Johnson, and L. Chapon, Magnetically-induced ferroelectricity in the  $(\text{ND}_4)_2[\text{FeCl}_5(\text{D}_2\text{O})]$  molecular compound, *Scientific Reports* **5**, 14475 (2015).
- [29] W. Tian, H. Cao, J. Wang, F. Ye, M. Matsuda, J.-Q. Yan, Y. Liu, V. O. Garlea, H. K. Agrawal, B. C.

- Chakoumakos, B. C. Sales, R. S. Fishman, and J. A. Fernandez-Baca, Spin-lattice coupling mediated multiferroicity in  $(\text{ND}_4)_2\text{FeCl}_5 \cdot \text{D}_2\text{O}$ , *Phys. Rev. B* **94**, 214405 (2016).
- [30] J. N. McElearney and S. Merchant, Nonisomorphic antiferromagnetic behavior of two isomorphous salts: low-temperature heat capacities and magnetic susceptibilities of diammonium iron pentachloride monohydrate and dipotassium iron pentachloride monohydrate, *Inorganic Chemistry* **17**, 1207 (1978).
- [31] D. Brüning, T. Fröhlich, M. Langenbach, T. Leich, M. Meven, P. Becker, L. Bohatý, M. Grüninger, M. Braden, and T. Lorenz, Magnetoelectric coupling in the mixed erythrosiderite  $[(\text{NH}_4)_{1-x}\text{K}_x]_2[\text{FeCl}_5(\text{H}_2\text{O})]$ , *Phys. Rev. B* **102**, 054413 (2020).
- [32] K. Momma and F. Izumi, *VESTA3* for three-dimensional visualization of crystal, volumetric and morphology data, *Journal of Applied Crystallography* **44**, 1272 (2011).
- [33] W. Tian, H. B. Cao, A. J. Clune, K. D. Hughey, T. Hong, J.-Q. Yan, H. K. Agrawal, J. Singleton, B. C. Sales, R. S. Fishman, J. L. Musfeldt, and J. A. Fernandez-Baca, Electronic phase separation and magnetic-field-induced phenomena in molecular multiferroic  $(\text{ND}_4)_2\text{FeCl}_5 \cdot \text{D}_2\text{O}$ , *Phys. Rev. B* **98**, 054407 (2018).
- [34] J. A. Rodríguez-Velamazán, O. Fabelo, J. Campo, J. Rodríguez-Carvajal, N. Qureshi, and L. C. Chapon, Switching of the Chiral Magnetic Domains in the Hybrid Molecular/Inorganic Multiferroic  $(\text{ND}_4)_2[\text{FeCl}_5(\text{D}_2\text{O})]$ , *Scientific Reports* **8**, 174439 (2018).
- [35] J. A. Rodríguez-Velamazán, O. Fabelo, J. Campo, A. Millán, J. Rodríguez-Carvajal, and L. C. Chapon, Magnetic-field-induced change of magnetoelectric coupling in the hybrid multiferroic  $(\text{ND}_4)_2[\text{FeCl}_5 \cdot \text{D}_2\text{O}]$ , *Phys. Rev. B* **95**, 174439 (2017).
- [36] K. Schmalzl, W. Schmidt, S. Raymond, H. Feilbach, C. Mounier, B. Vettard, and T. Brückel, The upgrade of the cold neutron three-axis spectrometer IN12 at the ILL, *Nuclear Instruments and Methods in Physics Research Section A: Accelerators, Spectrometers, Detectors and Associated Equipment* **819**, 89 (2016).
- [37] P. J. Brown, *Neutron scattering from magnetic materials* (Elsevier, Amsterdam, 2006) Chap. 5 - Spherical Neutron Polarimetry, pp. 215–244.
- [38] Y. Ishibashi and Y. Takagi, Note on ferroelectric domain switching, *Journal of the Physical Society of Japan* **31**, 506 (1971).
- [39] Y. Ishibashi, A model of polarization reversal in ferroelectrics, *Journal of the Physical Society of Japan* **59**, 4148 (1990).
- [40] M. Avrami, Kinetics of Phase Change. I General Theory, *The Journal of Chemical Physics* **7**, 1103 (1939).
- [41] M. Avrami, Kinetics of Phase Change. II Transformation-Time Relations for Random Distribution of Nuclei, *The Journal of Chemical Physics* **8**, 212 (1940).
- [42] M. Avrami, Granulation, Phase Change, and Microstructure Kinetics of Phase Change. III, *The Journal of Chemical Physics* **9**, 177 (1941).
- [43] D. Senff, P. Link, K. Hradil, A. Hiess, L. P. Regnault, Y. Sidis, N. Aliouane, D. N. Argyriou, and M. Braden, Magnetic Excitations in Multiferroic  $\text{TbMnO}_3$ : Evidence for a Hybridized Soft Mode, *Phys. Rev. Lett.* **98**, 28 (2007).
- [44] S. Holbein, P. Steffens, S. Biesenkamp, J. Ollivier, A. C. Komarek, M. Baum, and M. Braden, Spin-wave dispersion and magnon chirality in multiferroic  $\text{TbMnO}_3$  (2023), arXiv:2308.09407 [cond-mat.str-el].
- [45] X. Bai, R. S. Fishman, G. Sala, D. M. Pajeroski, V. O. Garlea, T. Hong, M. Lee, J. A. Fernandez-Baca, H. Cao, and W. Tian, Magnetic excitations of the hybrid multiferroic  $(\text{ND}_4)_2\text{FeCl}_5 \cdot \text{D}_2\text{O}$ , *Phys. Rev. B* **103**, 224411 (2021).
- [46] F. Kagawa, N. Minami, S. Horiuchi, and Y. Tokura, Athermal domain-wall creep near a ferroelectric quantum critical point, *The Journal of Chemical Physics* **7**, 10675 (2016).
- [47] J. Brooke, T. F. Rosenbaum, and G. Aeppli, Tunable quantum tunnelling of magnetic domain walls, *Nature* **413**, 610 (2001).
- [48] T. Finger, D. Senff, K. Schmalzl, W. Schmidt, L. P. Regnault, P. Becker, L. Bohatý, and M. Braden, Polarized-neutron-scattering studies on the chiral magnetism in multiferroic  $\text{MnWO}_4$ , *J. Phys. Conf. Ser.* **211**, 012001 (2010).
- [49] R. Kajimoto, H. Yoshizawa, H. Shintani, T. Kimura, and Y. Tokura, Magnetic structure of  $\text{TbMnO}_3$  by neutron diffraction, *Phys. Rev. B* **70**, 012401 (2004).
- [50] M. Kenzelmann, A. Harris, S. Jonas, C. Broholm, J. Schefer, S. Kim, C. Zhang, S.-W. Cheong, O. Vajk, and J. Lynn, Magnetic Inversion Symmetry Breaking and Ferroelectricity in  $\text{TbMnO}_3$ , *Phys. Rev. Lett.* **95**, 27 (2005).
- [51] S. B. Wilkins, T. R. Forrest, T. A. W. Beale, S. R. Bland, H. C. Walker, D. Mannix, F. Yakhov, D. Prabhakaran, A. T. Boothroyd, J. P. Hill, P. D. Hatton, and D. F. McMorrow, Nature of the Magnetic Order and Origin of Induced Ferroelectricity in  $\text{TbMnO}_3$ , *Phys. Rev. Lett.* **103**, 207602 (2009).
- [52] V. Scagnoli, S. W. Huang, M. Garganourakis, R. A. de Souza, U. Staub, V. Simonet, P. Lejay, and R. Ballou, Dzyaloshinskii-Moriya driven helical-butterfly structure in  $\text{Ba}_3\text{NbFe}_3\text{Si}_2\text{O}_{14}$ , *Phys. Rev. B* **88**, 104417 (2013).
- [53] Data are available at <https://doi.ill.fr/10.5291/ILL-DATA.CRG-2573>.